

On the geometry of the Orion Bar

WILLIAM J. HENNEY¹

¹*Instituto de Radioastronomía y Astrofísica, Universidad Nacional Autónoma de México, Apartado Postal 3-72, 58090 Morelia, Michoacán, Mexico*

Abstract

I critically examine different geometrical models that have been proposed for the geometry of the Orion Bar photodissociation region. From a re-analysis of the 21 cm H₁ observations, I show that the ionization front at the Bar must be convex, which rules out important classes of models. Furthermore, I show that small scale irregularities in the ionization front and dissociation front are important for analysing the apparent stratification and widths of different emission regions.

Keywords: Atomic physics; Radiative transfer; Photodissociation regions

1. REANALYSIS OF 21 CM H₁ OBSERVATIONS OF THE ORION BAR

Karl G. Jansky Very Large Array observations of the H₁ 21 cm line from the Orion Nebula and its surroundings at a spatial resolution of $\approx 6''$ and a velocity resolution of 0.77 km s⁻¹ were presented in ?, hereafter vDW13. The line is seen both in emission and absorption of the strong free-free continuum emitted by the ionized nebula. The majority of the absorption arises in the foreground Veil at Local Standard of Rest velocities of $v_{\text{lsr}} = -2 \text{ km s}^{-1}$ to 7 km s⁻¹. Emission is seen primarily at more redshifted velocities of 10 km s⁻¹ to 15 km s⁻¹, similar to the velocities of the molecular gas seen in CO, although at large distances from the center of the nebula the Veil is also seen in emission. The analysis of the absorption components by vDW13 was carried out under the assumptions that (i) all of the continuum emission arises from *behind* the absorbing H⁰ column (from the point of view of the Earth), and (ii) line emission is negligible at velocities where absorption is detected. These are both very good assumptions in the case of absorption by the foreground Veil, but they break down for the case of the Orion Bar, where both emission and absorption are seen at similar velocities and in spatially adjacent regions. Given the wealth of information on the physical conditions and geometry that these data provide, it is worth reanalyzing them under less restrictive assumptions.

Figure 1. Three-layer sandwich structure for H₁ 21 cm radiative transfer.

w.henney@irya.unam.mx

In the Rayleigh–Jeans limit, the frequency-dependent surface brightness I_ν is characterized by the brightness temperature in each velocity channel: $T_b(v) = c^2 I_\nu / 2k\nu^2$, where $v/c = (\nu/\nu_0) - 1$ and $\nu_0 = 1.420\,405 \text{ GHz}$. The radiative transfer equation can be solved for an idealized three-layer sandwich structure (see Fig. ??), consisting of (1) a background H⁺ region with electron temperature T_e and free-free continuum optical depth τ' , (2) an intermediate neutral H⁰ layer with spin temperature T_s and line optical depth $\tau(v)$, and (3) a foreground H⁺ region with the electron temperature T_e and free-free continuum optical depth τ'' . The continuum source function in regions 1 and 3 is T_e , whereas the line source function in region 2 is T_s . Region 2 is assumed to have zero continuum optical depth. Following vDW13, large-scale Milky Way H₁ line emission along the line of sight through Orion is neglected since it is (a) very faint compared with the nebula, with $T_b(v) < 48 \text{ K}$ at $v = 10 \text{ km s}^{-1}$ (??), and (b) any emission that is smooth on angular scales below 7 arcminutes will be filtered out by the interferometer.

At continuum frequencies just off the line, $\tau(v) = 0$ and only regions 1 and 3 contribute to the observed brightness, yielding a continuum brightness temperature

$$\begin{aligned} T_c &= T_e \left(1 - e^{-(\tau' + \tau'')} \right) \\ &= T_c' e^{-\tau'} + T_c'' , \end{aligned} \quad (1)$$

where the second equality gives the decomposition into separate contributions from region 1: $T_c' = T_e(1 - e^{-\tau'})$, and region 3: $T_c'' = T_e(1 - e^{-\tau''})$. At frequencies where the line opacity is significant, all three regions contribute, yielding

$$T_b(v) = T_c' e^{-(\tau(v) + \tau'')} + T_s \left(1 - e^{-\tau(v)} \right) e^{-\tau''} + T_c'' . \quad (2)$$

For practical reasons related to the deconvolution of the interferometric data, the results of vdW13 are presented in continuum-free form as $\tilde{T}_b(v) = T_b(v) - T_c$. Combining equation (??) and (??), one finds

$$\tilde{T}_b(v) = [1 - e^{-\tau(v)}] [1 - (T_c''/T_e)] [T_s - T_c'] . \quad (3)$$

The relative brightness temperature of the line, $\tilde{T}_b(v)$, is therefore seen to be the product of three factors, given by the three sets of square brackets in equation (??). The first two factors are always positive since $\tau(v) \geq 0$ and $T_c'' \leq T_e$, but the third factor can take either sign. When the continuum brightness temperature T_c' of the background photoionized gas in region 1 exceeds the spin temperature T_s of neutral hydrogen in region 2, then we see an absorption line: $\tilde{T}_b(v) < 0$. On the other hand, when T_s is higher than T_c' , then we see an emission line: $\tilde{T}_b(v) > 0$. In either case, the maximum line strength will be found when region 2 is opaque ($\tau(v) \gg 1$) and region 3 is transparent ($T_c'' \ll T_e$), yielding $\max(|\tilde{T}_b(v)|) = |T_s - T_c'|$.

The electron temperature in the ionized gas is expected to be roughly constant at $T_e \approx 11\,000$ K (?), but this still leaves 4 unknown quantities, $\tau(v)$, T_s , T_c' , and T_c'' , to be determined from 2 observed quantities: T_c and $\tilde{T}_b(v)$. Further assumptions must therefore be made in order to interpret the observations, but these can be guided by the observed spatial trends and simple geometric models. For instance, in the Orion Bar the free-free continuum brightness temperature falls sharply across the ionization front from $T_c \approx 3000$ K on the ionized side, but then levels off to a roughly constant value of $T_c \approx 600$ K on the neutral side. Assuming that this constant value reflects unrelated foreground emission (probably ionized by θ^2 Ori A) that overlays the entire Bar (this hypothesis is tested

below), we have an upper limit to the background emission of $T_c - 600$ K. It can be further assumed that the emission from region 1 is a constant fraction, f_{bg} , of this upper limit:

$$T_c' = f_{bg}(T_c - 600 \text{ K}) . \quad (4)$$

If the Bar geometry is a cylinder that is illuminated from the side (see Fig. XXX), then $f_{bg} = 0.5$ is appropriate. If the Bar is illuminated from slightly behind, or if it is an escarpment, or if an additional background component is present (see § ??), then the fraction will be larger: $0.5 < f_{bg} < 1.0$.

Further progress can then be made by considering null points in the nebula where line emission and absorption cancel out. At such points $\tilde{T}_b(v) \approx 0$, so that $T_s = T_c'$ by equation (??). Absorption component M is identified by vdW13 as associated with H⁰ in the Bar, due to its velocity and spatial distribution. Component M consists of a string of knots with $\tilde{T}_b(v) = -200$ to -400 K at $v \approx 11 \text{ km s}^{-1}$. They are arranged parallel to the Bar, just behind the ionization front at a relative position of roughly 0.006 pc (see Fig. ??) and where the continuum brightness has fallen to $T_c \approx 2200$ K. At greater distances from the ionization front the H₁ at this velocity is seen in emission, reaching a peak of $\tilde{T}_b(v) \approx 250$ K at 0.030 pc where $T_c \approx 750$ K. The crossover null point where $\tilde{T}_b(v) = 0$ occurs between these two at 0.012 pc where $T_c \approx 1500$ K.

Add a table showing

1.1. Structure of the Orion Bar

1.1.1. Cloudy model predictions for the optical depths

In order to investigate the role of dust extinction in greater detail in more detail the

Maybe ditch this section

REFERENCES

- Bally, J., O'Dell, C. R., & McCaughrean, M. J. 2000, AJ, 119, 2919, doi: [10.1086/301385](https://doi.org/10.1086/301385)
- Dicker, S. R., Mason, B. S., Kornget, P. M., et al. 2009, ApJ, 705, 226, doi: [10.1088/0004-637X/705/1/226](https://doi.org/10.1088/0004-637X/705/1/226)
- Foster, J. B., & Goodman, A. A. 2006, ApJL, 636, L105, doi: [10.1086/500131](https://doi.org/10.1086/500131)
- Goicoechea, J. R., Pety, J., Cuadrado, S., et al. 2016, Nature, 537, 207, doi: [10.1038/nature18957](https://doi.org/10.1038/nature18957)
- Green, D. A. 1991, MNRAS, 253, 350, doi: [10.1093/mnras/253.2.350](https://doi.org/10.1093/mnras/253.2.350)
- Green, D. A., & Padman, R. 1993, MNRAS, 263, 535, doi: [10.1093/mnras/263.2.535](https://doi.org/10.1093/mnras/263.2.535)
- Kissler-Patig, M., Pirard, J. F., Casali, M., et al. 2008, A&A, 491, 941, doi: [10.1051/0004-6361:200809910](https://doi.org/10.1051/0004-6361:200809910)
- van der Werf, P. P., Goss, W. M., & O'Dell, C. R. 2013, ApJ, 762, 101, doi: [10.1088/0004-637X/762/2/101](https://doi.org/10.1088/0004-637X/762/2/101)

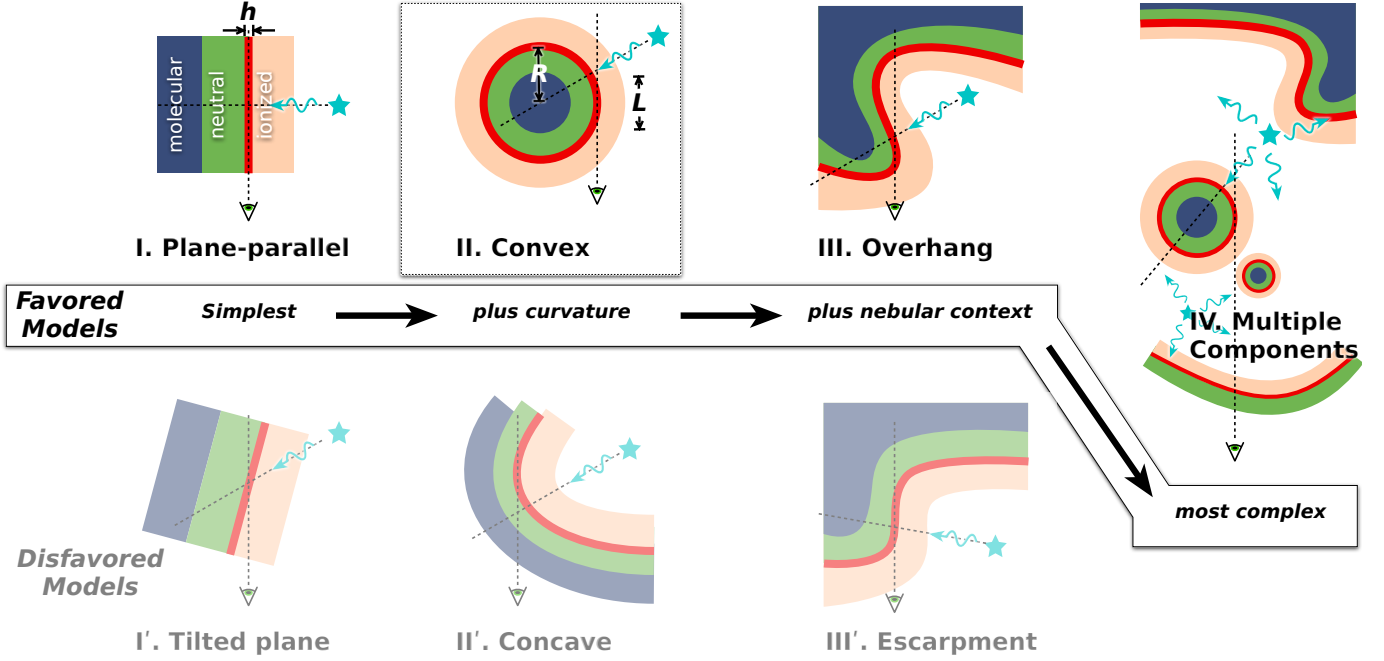


Figure 2. Different classes of geometrical models that have been proposed for the Orion Bar. The sequence of models I, II, III, IV are of increasing complexity, but also increasing scope and explanatory power. Models I', II', III', on the other hand, are disfavored due to either underperformance or falsification (see text for further details). For all models, dark blue shading represents molecular gas, green shading represents neutral gas, and light orange shading represents ionized gas. An example emission layer of thickness h and radius of curvature R is indicated by thick red lines. The line-of-sight depth of the emission layer is denoted by L . The direction of illumination and the line of sight are indicated by thin dotted lines.

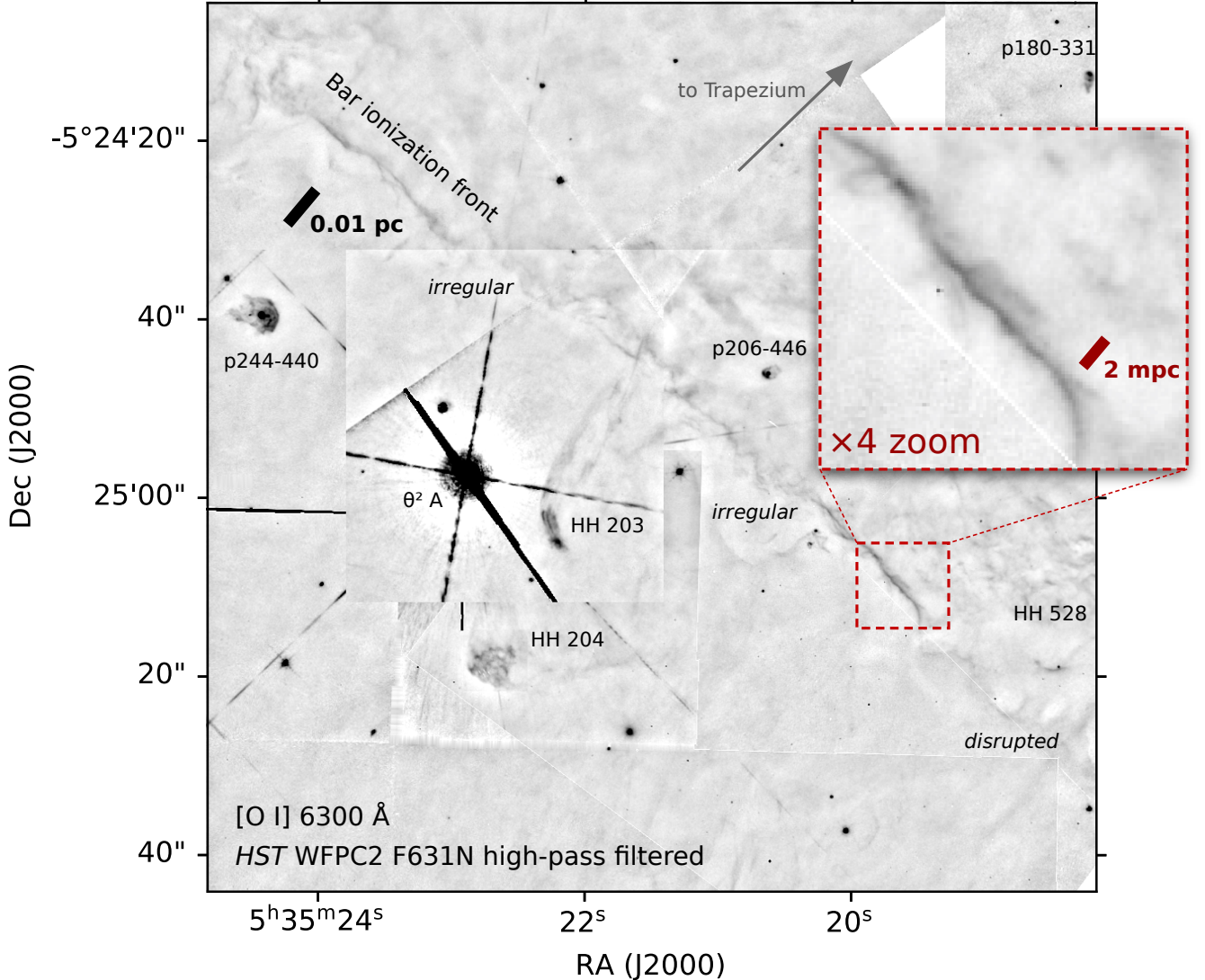


Figure 3. Fine-scale structure of the ionization front at the Orion Bar. Grayscale image shows a $90'' \times 90''$ section of a mosaic of *HST* WFPC2 observations (?) in the F631N filter, which mainly passes the [O I] 6300 Å line. The image has been high-pass filtered to remove large-scale brightness gradients (> 16 arcsec). The principal ionization front of the Bright Bar runs diagonally from top-left to bottom-right. It can be seen that the front is very irregular on scales of 1 to 10 mpc, and even becomes disrupted completely in some segments. Only in a few places is the front straight and regular enough for its true sharpness to be seen, such as the small area shown in a zoomed box, where the width of the [O I] ridge can be seen to be less than 1 mpc. Apart from the Bright Bar ionization front, other fine-scale features visible in the image are associated with Herbig–Haro jets and proplyds.

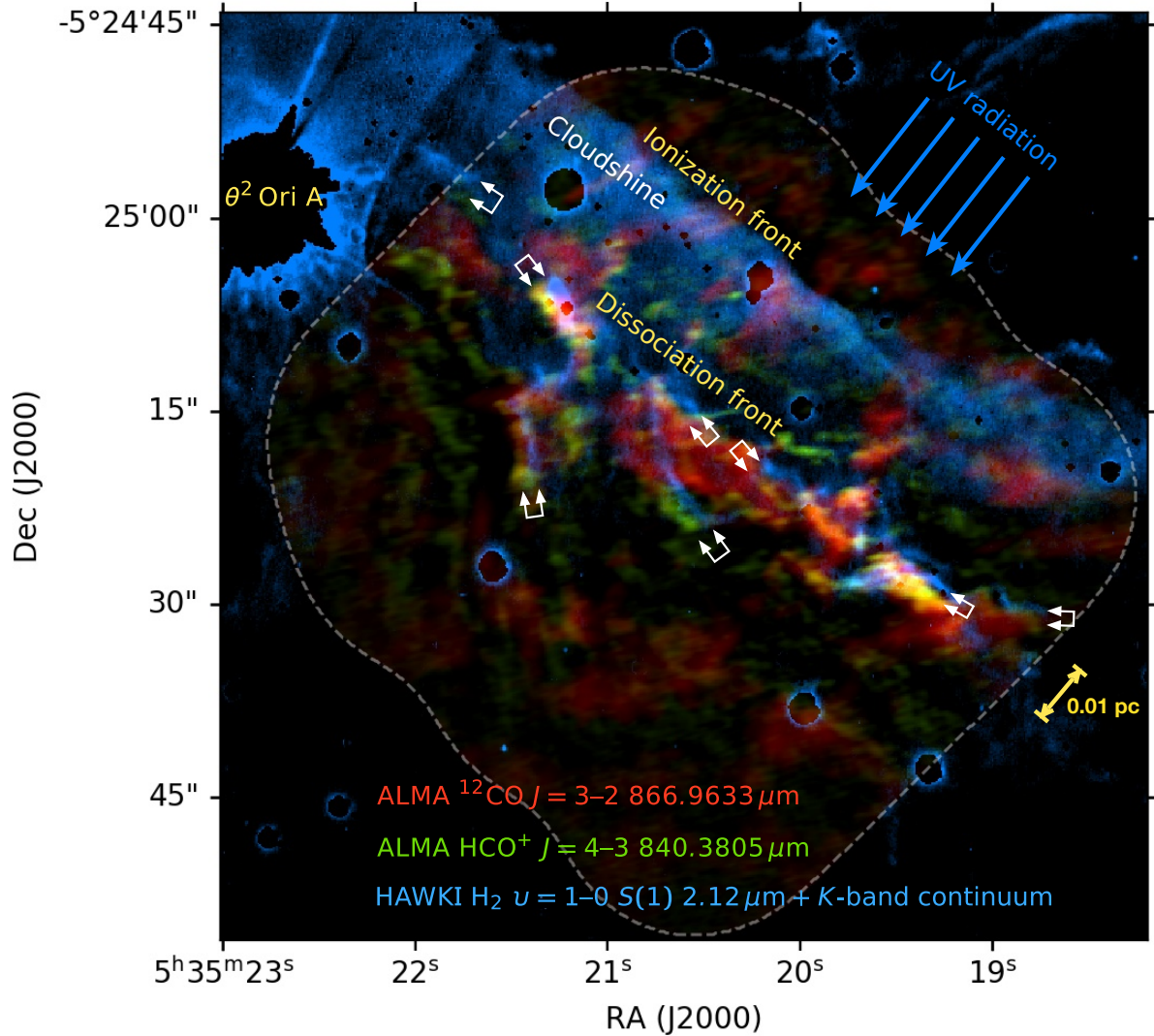


Figure 4. Fine-scale structure of the dissociation front in the Orion Bar. Double white arrows mark out some instances of stratification between emission of H_2 (blue) and heavier molecules (green/yellow/red). In every instance H_2 is displaced towards the irradiated side of the filament by $1''$ to $2''$ (≈ 0.003 pc). Background image shows ALMA mosaics (?) of the sub-mm CO $J = 3 \rightarrow 2$ 866.96 μm HCO^+ 840.38 μm emission lines in the red and green color channels, respectively, with the boundary of the ALMA field shown by the gray dashed line. The blue color channel of the background image shows near-infrared vibrationally excited H_2 $v = 1 \rightarrow 0$ $S(1)$ 2.12 μm emission, extracted from narrow-band imaging with ESO's High Acuity Wide-field Imager (HAWK-I, ?). The H_2 image has been corrected for contamination by ionized emission (mainly hydrogen Brγ recombination line), but has not been continuum-subtracted. As a result, scattered starlight (cloudshine, ?) is seen as a band of diffuse emission that falls off smoothly behind the ionization front.

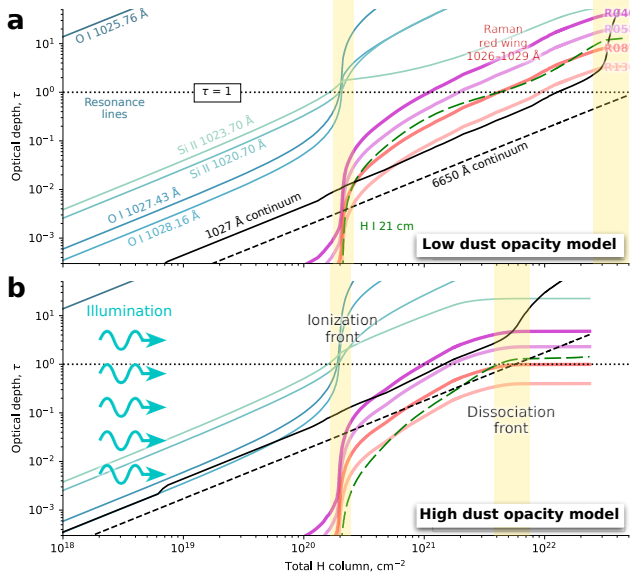


Figure 5. Optical depth of select processes as a function of total hydrogen nucleon column density, calculated from static Cloudy simulations of the Orion Bar. All optical depths and columns are measured with respect to the illuminating Trapezium stars, which are situated to the left in this figure. Separate panels show two models that differ only in the assumed dust absorption opacity: (a) low opacity, $\sigma_{\text{FUV}} \approx 5 \times 10^{-23} \text{ cm}^2 \text{ H}^{-1}$, and (b) high opacity, $\sigma_{\text{FUV}} \approx 5 \times 10^{-22} \text{ cm}^2 \text{ H}^{-1}$. Optical depths of O^0 and Si^+ absorption lines in the Ly β wings are shown in blue. Continuum optical depths near Ly β (solid line) and H α (dashed line) are shown in black. The H 0 21 cm line optical depth is shown in green (long dashed line). Optical depths to Rayleigh/Raman scattering for 4 observed bands in the red wing of Ly β (see Table ??) are shown in red.

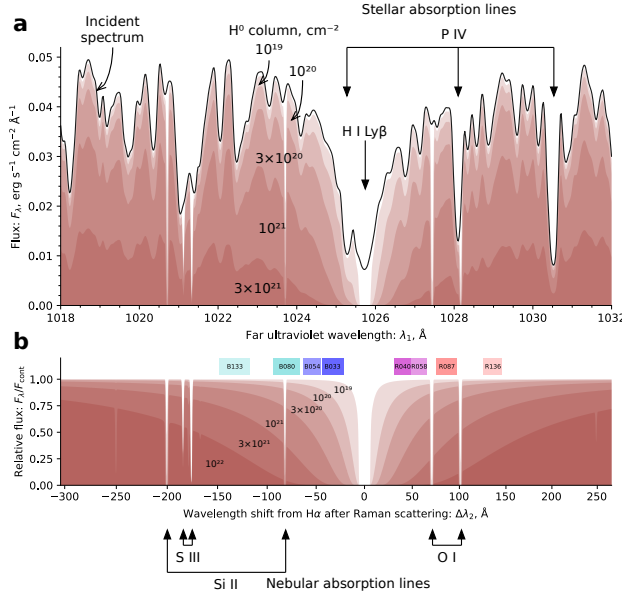


Figure 6. (a) Predicted spectrum of Trapezium stars in vicinity of Ly β from POWR OB atmosphere models (black line), together with attenuation by Cloudy model of the Orion Bar (red filled shapes), extracted at a series of values of the neutral hydrogen column density, as marked. (b) Relative attenuation of the incident spectrum by line opacity only (that is, neglecting dust continuum opacity) in the Cloudy models, which shows the development of the Ly β damping wings as the column density increases. In this panel, the x axis is labelled with $\Delta\lambda_2$ in the optical domain, allowing direct comparison with the observations presented in Figure ?? (observed Raman bands are indicated by colored boxes). Note that the scale is linear in λ_1 , which is slightly non-linear in $\Delta\lambda_2$. Wavelengths of some of the more prominent stellar photospheric lines and nebular absorption lines are marked.